

Design of a Communications System for Advanced CubeSat Missions

Cameron Phillips

Abstract—Advancements in miniaturised electric propulsion systems are enabling CubeSats to perform advanced orbital manoeuvres. CubeSat communications systems must be capable of adapting to these changing conditions, ensuring a reliable data link is maintained whilst adhering to a low power budget. This paper presents a baseline on the performance of the communications system for these potential missions. A high-gain phased patch antenna array operating within the X-band is designed and presented for the proposed missions. A channel model of the 10.475 GHz satellite-Earth link is created to evaluate the performance of binary phase shift keying (BPSK) modulation and error-correcting turbo codes. Simulations of the overall performance at varying orbits are used to determine the feasibility of such missions. Results from these simulations demonstrated that a 10.475 GHz communications system using a 4x4 phased planar antenna array, BPSK modulation, and turbo coding was capable of maintaining a reliable link throughout the CubeSat’s mission using 1 W of power.

I. INTRODUCTION

THE commercialisation of space saw the introduction of many large-scale communications satellites operating from Medium Earth Orbit (MEO) to Geostationary Orbit (GEO). These satellites had powerful yet bulky communications systems, enabling high data throughput to and from ground stations. Recent improvements in satellite technology allowed for a significant size reduction, which saw the introduction of a new class of satellites called CubeSats. This class typically operates in Low Earth Orbit (LEO) and provides an alternative to the expensive and bulky satellites operating at greater altitudes. CubeSats consist of specified units, with 1U being defined as 10 cm × 10 cm × 10 cm. To be classified as a CubeSat, the satellite must comprise these defined units; therefore, these satellites have restricted capabilities.

Low-power communication becomes problematic at increasing altitudes due to significant attenuation introduced by the channel. CubeSats are typically placed in LEO; thus, this constraint did not significantly impact their operation. However, with improvements in low-power electric propulsion systems, these satellites are being introduced at higher altitudes. New electric propulsion systems are allowing CubeSats to perform advanced orbital manoeuvres, taking them from LEO to GEO, that is, increasing their altitudes from 500 km up to 35,786 km in a single mission [1]. Communications systems onboard these satellites must adapt to changes in altitudes and operate reliably throughout the mission.

Elevated orbits demand high-gain antennas for reliable communication. This requires focused antenna beams, which

makes maintaining coverage at lower altitudes more challenging due to narrow beamwidths attributed to high-gain antennas. Narrow beamwidths do not impact coverage at high altitudes due to the beam’s extended projection on the Earth’s surface.

The influence of Earth’s gravity on spacecraft velocities varies with altitude. Velocities at LEO are typically around 8 km/s, and 3.0 km/s at GEO. Resultingly, satellites operating in LEO pass over any given point on Earth far more rapidly than those operating at higher altitudes. The satellite’s radial velocity matches that of Earth at GEO, therefore it remains at the same projected point on Earth throughout its orbit. This presents a significant contrast between altitude limits. At GEO the CubeSat is predominantly over New Zealand and requires a narrow beamwidth to maximise gain. It is not constrained by link time, allowing lower data rates to be used. In contrast, CubeSats operating in LEO have limited link time due to reduced coverage imposed by low altitudes and rapid flyovers. Wide beamwidths and high data rates are typically used to circumvent these constraints.

Victoria University of Wellington (VUW) is proposing a mission that leverages newly developed electric thruster technology to propel a CubeSat from LEO to GEO in a circular orbit over a 100-day mission [1]. The key objective of the mission is to take measurements of the Earth’s magnetic field as the CubeSat is propelled from LEO to GEO. The sampled data is to be taken at a resolution of one sample per km in orbit, where each sample consists of four scalar quantities, each quantised to 16 bits. A communications system is required to transmit this data to a ground station based at VUW in Wellington, New Zealand. Crucial telemetry data and key scientific data being transferred from the CubeSat to the ground station must be received with a minimal bit error rate (BER) to ensure data integrity. Where a low BER cannot be achieved, error-correcting techniques, such as automatic repeat request (ARQ) and forward error correcting (FEC), are required to circumvent errors. A scheme that ensures data integrity is maintained, regardless of the BER, is considered a success for this mission.

A model of the end-to-end communications system for the proposed mission is required to quantify attainable data throughput and to provide mission planners with an understanding of achievable mission goals. This includes describing an antenna system, investigating the impact on signals as they pass through Earth’s atmosphere, and exploring techniques to encode signals that maximise throughput. A realistic understanding of available communication link times can be gained by simulating an orbit that maximises coverage of New Zealand.

This project was supervised by Pawel Dmochowski (primary), Christopher Hollit (secondary).

A low-power patch antenna phased array operating in X-band with a resonant frequency of 10.475 GHz is proposed to allow CubeSats to reliably send and receive data when operating at GEO. Furthermore, the performance of FEC turbo codes, along with BPSK and binary frequency shift keying (BFSK) modulation schemes are investigated and discussed. A successful communications system will be able to reliably deliver the CubeSat's payload at all of the described altitudes, whilst fitting the low-power requirements that CubeSats are constrained to. A target for this project is for the CubeSat's communications system to deliver all required data whilst using only 1 W of power.

Ensuring a reliable communications system is essential to minimising space junk around Earth. The onboard communications system is the only way crucial telemetry commands and data can be sent to and from the CubeSat, meaning that if the system fails the CubeSat itself would fail and would add to the steadily growing number of discarded satellites in orbit [2].

The aim of this project is to investigate and provide a model of an end-to-end communications system that looks to solve the issues described above. It is intended to provide a baseline for the CubeSat, which can be further refined depending on mission objectives. In essence, the project aims to:

- 1) Develop a model of an antenna system for a CubeSat that meets the size constraint of 10 cm \times 10 cm and provides reliable communication with a ground station from LEO to GEO.
- 2) Due to the CubeSat's limited resources, the overall communications system must use minimal power whilst still delivering the mission's payload requirements.
- 3) Obtain a mathematical model of the satellite-Earth link that signals will be propagating through. This is the channel model and will be used to accurately determine what coding techniques maximise performance.
- 4) Discuss the performance of the overall system utilising FEC turbo codes to ensure the integrity of key scientific data is maintained during transmission to the ground station.
- 5) Use appropriate tools to simulate the complete communications system in operation. This is to provide a benchmark for future revisions of the communications system.

II. ANTENNA SYSTEM BACKGROUND

A. Antenna Parameters

1) *Resonant Frequency*: An antenna's resonant frequency is where it operates most efficiently. Antennas are typically designed to resonate within a specific frequency band. The dimensions of an antenna are closely related to where the antenna resonates. This is because the dimensions are proportional to the wavelength of the intended operating frequency.

2) *Gain*: The gain of an antenna is the ratio of the radiation intensity in a given direction to the radiation intensity that would be obtained if the radiator was an isotropic antenna. This is a theoretical antenna that radiates equally in all directions. It is measured in decibels relative to isotropic, dBi, and

is a useful performance measure in satellite communications as it provides insight into how focused the radiating beam is. More focused beams have their energy concentrated over a smaller area, which is advantageous for communication systems operating over vast distances.

The gain of an antenna varies considerably depending on the antenna type. Monopole antennas have little directivity and tend to radiate uniformly in all directions, giving them a relatively small gain. Whilst this radiation pattern has been used for CubeSats in LEO [3], it becomes problematic for CubeSats in GEO whose signals undergo substantial attenuation with limited power resources. Patch antennas have more focused beams and therefore higher gains, making them more advantageous over monopole antennas.

The main lobe of an antenna is the beam with the maximum gain. A directional antenna's boresight is defined as the axis of maximum gain, which is typically perpendicular to the antenna.

3) *Polarisation*: The polarisation of an electromagnetic wave describes the time-varying direction and magnitude of the electric field vector observed along the propagation direction. Polarisation can be broken down into three primary categories: Linear, Circular, and Elliptical. Linear polarisation describes a wave whose electric field vector is only varying its direction along a single plane. Circular and Elliptical polarisation describes waves whose electric field vector rotates around a given axis as the wave propagates. The axial ratio (AR) of an antenna is the ratio between the major and minor axis of the rotating electric field. An AR of 0 dB describes perfect circular polarisation; anything above this value tends towards elliptical polarisation. An antenna must have an AR of < 3 dB to be defined as having circular polarisation.

Circularly polarised antennas can receive signals with different polarisations more effectively than linearly polarised antennas. This makes them less sensitive to polarisation alignment and avoids the issues caused by cross-polarisation (which is an unwanted change of a signal's polarisation that occurs as it propagates through a given medium) [4]. Patch antennas can be designed to have circular polarisation, so they are commonly used in applications where the antenna orientation cannot always be easily predicted, or in scenarios where cross-polarisation is likely [4]. Satellite communications systems that do not employ a circularly polarised antenna are required to be orientated in a particular way for communication to occur. Avoiding this requirement would be beneficial to the proposed mission as it mitigates events where valuable link time cannot be utilised due to incorrect satellite orientation.

4) *Reflection Coefficient*: Reflections within a circuit become a significant design consideration at high frequencies. The S_{11} reflection coefficient, measured in dB, describes the amount of the input signal that is reflected back from the input port and does not get absorbed by the load. This is predominantly caused by mismatched impedances between the input and the load. These reflected waves combine with source waves constructively and destructively to create standing waves, which creates inefficiencies and should be avoided. An ideal port that absorbs the entire signal is characterised by a reflection coefficient of 0 dB.

5) *Beamwidth*: The 3 dB beamwidth is the angle from the centre of the main lobe where the gain falls 3 dB from its maximum value. This provides a description of where a majority of a signal's energy is focused. A narrow 3 dB beamwidth results in a focused beam that has increased gain but covers less area, with a wide 3 dB beamwidth providing the inverse. Communication satellites are typically placed in a fixed orbit; as such, their beamwidth can be designed for a specific altitude. Satellites with varying orbits must adopt methods to provide coverage during all stages of a mission.

B. Planar Antennas

Planar antennas are fabricated on a printed circuit board (PCB) and consist of a radiating layer on the top, and a ground plane on the bottom, which are separated by a dielectric material known as the substrate. Planar antennas are low-profile and low-cost, making them suitable for CubeSat applications. Planar antennas designed to resonate at high frequencies (GHz) can be reduced to just a few centimeters in length. A patch antenna is a type of planar antenna that is commonly used in CubeSat applications operating at high frequencies [3].

The small form factor of the individual planar antennas allows them to be easily scaled to arrays, which provides increased gain, and can incorporate a phased array for electronic beam steering. Though arrays can be constructed from other antenna types, they are typically bulky and require deployment after launch to ensure they fit within the defined CubeSat dimensions during the launch phase [3]. Planar antenna systems do not require deployment, which decreases complexity and reduces the risk of failure after launch. Given the vital role that communication plays in all space missions, failure to deploy the antenna system would immediately end the mission.

C. Antenna Array

Planar antennas are seldom used on their own in satellite communications due to their low gain [5]. They are instead combined and used to create an array of antennas (elements) that has enhanced gain and directivity. Due to their small size, planar antennas are easily multiplied on a PCB into large arrays. Combining elements into an array creates a more directive beam due to waves from individual elements constructively and destructively interfering. This effect can be employed to steer the beam in various directions by controlling the phase of each element. An array that uses this principle is referred to as a phased array. This feature becomes particularly useful during rapid flyovers in LEO as steering the beam maximises available link time.

D. Existing Solutions

Inspection of literature provided an overview of various X-band antenna types and optimisation methodologies concerned with minimising the S_{11} reflection coefficient and AR, and maximising gain. Among the reviewed types, planar antennas were identified as the most suitable for CubeSat applications owing to their compact form factor which does not require

deployment [3]. A study of several X-band planar antennas demonstrated that the S_{11} parameter can be minimised to values between -40 dB and -13 dB, with the antennas exhibiting ARs of less than 3 dB. The operational gains of these antennas ranged from 7.2 dBi to 20.03 dBi.

The design methodology for an X-band planar antenna phased array was demonstrated to achieve circular polarisation using a truncated corner technique [6]. A transmission-line model¹ was implemented to design a single antenna, which was extended to a 16-element array. The design achieved an S_{11} value of -26.5 dB, and an AR of 2.34 dB. Whilst this methodology describes the design of a planar array operating at 8.21 GHz, it can be adapted for planar antennas operating at similar frequencies.

Horn antennas pose as an alternative to planar antennas, considered advantageous for their operational high-gain [7]. Although able to achieve circular polarisation and gains over 15 dBi, the bulky configuration prohibits their extension to arrays. As such, horn antennas must rely on mechanical systems for beam steering, which introduces a significant failure point in the communications system.

The described antennas have been deployed on CubeSats operating in LEO. They are untested for deployments at elevated orbits and thus require further investigation. The antenna parameters described provide a benchmark for this project, which can then be tested for orbital requirements stated in I. The planar antenna transmission-line model can be incorporated to facilitate this design.

III. ANTENNA DESIGN

A. Operating Frequency

An operating frequency was selected from available bands for amateur satellite service, which includes 144-146 MHz, 3.40-3.41 GHz, 10.45-10.50 GHz, 24.00-24.25 GHz, and many bands above this frequency [8]. As described in section II-B, planar antennas offer considerable benefits over alternative antenna types; especially when considering the constraints discussed in section I. Therefore, an operating frequency that allows full use of these antennas must be used.

The 144-146 MHz band cannot be used as the planar antenna would be too large to fit within the dimensions of the CubeSat due to the requisite wavelengths. A deployable antenna system will not be considered due to the complexity and excessive points of failure. Frequencies in the GHz range are more suitable for this communications system, however, careful consideration must be taken due to increased atmospheric attenuation at high frequencies [9]. A band in the low GHz is suitable for this antenna as it will have a wavelength small enough for a planar antenna, and will face minimal attenuation as it passes through the atmosphere (discussed further in Section IV-B). 10.45-10.50 GHz is selected with a centre frequency of 10.475 GHz as it offers a wider bandwidth compared to the other available band (3.40-3.41 GHz) and has a smaller wavelength of 3 cm (compared to 9 cm), resulting in a smaller element.

¹A common design methodology for planar antennas [5].

B. Element Design

The design of the patch antenna is analysed through the transmission-line model. This model is simple and provides insight into the physical patch element [5]. The transmission-line model represents the antenna as two radiating apertures, each with width, W , height, h , separated by a distance, L .

Because a dielectric material separates the radiating layer and the ground plane, the electric field lines at the edges of the patch will undergo fringing due to the element's finite length [5]. The fringing effect is the bending of the electric field lines at the edges of the radiator, which creates a variation in the intensity of the electric field. Consequently, the resonant length of the patch will not match its physical length, as shown in Figure 1. As a result, the effective length, L_{eff} , and effective dielectric constant, ϵ_{eff} , due to fringing must be considered. Key antenna parameters, such as resonance, are sensitive to the effective length of the patch.

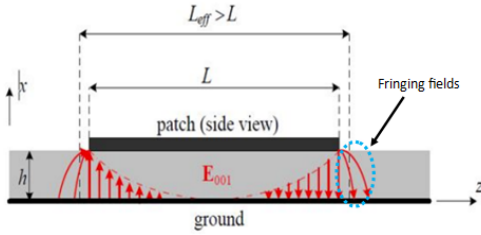


Fig. 1. Fringing effect on a patch antenna (shown in blue) [10].

To calculate the effective dimensions using the transmission-line model, the effective dielectric constant must be calculated using [5]

$$\epsilon_{\text{reff}} = \frac{\epsilon_r + 1}{2} + \frac{\epsilon_r - 1}{2} \left[1 + 12 \frac{h}{W} \right]^{-\frac{1}{2}} \quad (1)$$

where ϵ_r is the dielectric constant of the substrate. The width, W , can then be calculated using

$$W = \frac{\nu_0}{2f_r} \sqrt{\frac{2}{\epsilon_r + 1}} \quad (2)$$

where ν_0 is the free-space velocity of light and f_r is the resonant frequency of the antenna. The resonance of the antenna is based on its effective length, L_{eff} , therefore, to correctly size a patch antenna the effective length of the patch must be used, which can be found using

$$L_{\text{eff}} = L + 2\Delta L \quad (3)$$

where ΔL can be found using

$$\Delta L = 0.412h \frac{(\epsilon_{\text{reff}} + 0.3) \left(\frac{W}{h} + 0.264 \right)}{(\epsilon_{\text{reff}} - 0.258) \left(\frac{W}{h} + 0.8 \right)} \quad (4)$$

The extensions of the patch electrically due to fringing, ΔL , can be subtracted from L_{eff} to find the required length of the patch, L , that is

$$L = \frac{1}{2f_r \sqrt{\epsilon_{\text{reff}} \sqrt{\mu_0 \epsilon_0}}} - 2\Delta L \quad (5)$$

where μ_0 and ϵ_0 are the permeability and permittivity of free space respectively.

As mentioned in Section II-A3, circularly polarised antennas are able to more effectively receive signals regardless of their orientation. As such, the discussed patch antenna employs truncated corners to achieve circular polarisation, which enables two orthogonal modes with a 90° phase difference to be excited [11]. The truncated corners were arbitrarily set to $S = 1$ mm before being optimised in CST Studio 2022².

The Rogers RT5880 substrate is selected as the dielectric material between the radiating layer and the ground layer. The height and dielectric constant of the selected substrate are important considerations when designing the patch antenna. This substrate comes with a standard height of 1.575 mm and has a dielectric constant of 2.20. A source of inefficiency in this type of antenna is caused by the excitation of surface waves, which are parasitic waves that propagate through the substrate [12]. As the substrate's dimensions are finite, the surface waves will radiate out as they meet its edges - shown in Figure 2. This increases cross-polarisation, which degrades the antenna's intended polarisation. Furthermore, the radiating surface waves deform the antenna's radiating pattern. Surface waves can be minimised by decreasing the thickness of the substrate as less energy will be coupled into the surface waves. However, a balance must be found as decreasing the substrate also reduces antenna bandwidth and efficiency [12]. In [6], an X-band patch antenna was designed that achieved reasonable gain and efficiencies using the RT5880 substrate; therefore, this was selected for this communications system.

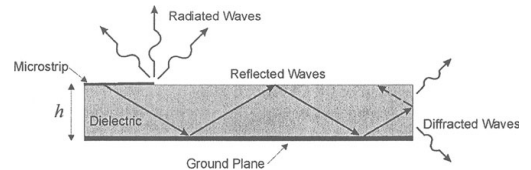


Fig. 2. Effects of surface waves through the substrate [12].

The transmission-line model design procedure can now be utilised to calculate the required dimensions for the patch antenna. The design procedure is as follows:

- 1) Find the width, W , of the patch antenna using (2).
- 2) Calculate the effective dielectric constant, ϵ_{reff} , using (1).
- 3) Find the electrical extension of the length, ΔL , due to fringing using (4).
- 4) Find the physical length, L , of the patch using (5).

Using $\epsilon_r = 2.20$, $h = 1.575$ mm, and $f_r = 10.475$ GHz the dimensions of the patch can be found using the equations above. They were found to be $W = 11.3$ mm and $L = 8.6$ mm. Equal sides of the patch must be maintained to achieve circular polarisation through the truncated corner method. As the width of the patch is not a crucial design parameter, it was adjusted to match the length [13]. This results in $W = 8.60$ mm

²CST Studio 2022 is a widely used software package for electromagnetic simulation

and $L = 8.60$ mm. These dimensions were then optimised in CST Studio.

C. Element Feeding Method

Impedance matching in high-frequency circuits is essential for maximising the power being absorbed by the load. The feeding method describes the technique used to match the impedances of the transmission line and the antenna. Reflections at junctions will occur if the impedance is not matched. A feeding method that minimises this must be utilised to preserve system efficiency.

Three commonly employed feeding methods are coaxial feed, inset feed, and quarter wavelength feed. Each method has its respective benefits and drawbacks, such as ease of fabrication and resulting gain: a balance between these factors must be found for a specific application. The three described methods are investigated to determine which best meets the requirements in Section II-D.

Coaxial feeds employ a coax connector that is placed on the ground plane, with a probe fed through the substrate to the radiator via the coaxial cable's core conductor. The outer layer of the coax is connected to the ground plane. Impedance matching can be accomplished by adjusting the probe's position on the patch [5]. Whilst this feeding technique is simple to model, it can be costly to fabricate and cannot be easily extended to an array.

An inset feed involves inserting the microstrip transmission line further up the patch. When a patch antenna is excited, the current on the edge of the patch is zero and is maximised at its centre. This means the impedance is maximum at the edges and minimum at the centre. By adjusting the inset position the impedance of the feed can be adjusted to match the microstrip transmission line [14]. A drawback to the inset feed is that the cutout slot creates coupling capacitance between the patch and the feed line, which shifts the resonant frequency by $\sim 1\%$ [13].

A quarter wavelength feed (also known as a quarter wavelength transformer) involves varying the transmission line's width for a length of $\frac{\lambda}{4}$ to adjust its impedance. This technique is cost-effective and easy to model as it only requires adjustments to the transmission line's width. The required impedance of the quarter wavelength transformer is found using

$$Z_{0T} = \sqrt{Z_1 Z_2} \quad (6)$$

where Z_1 and Z_2 are the impedances being matched. The quarter wave transformer being calculated can be seen in Figure 3.

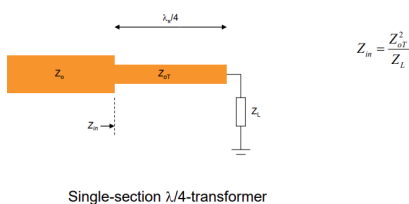


Fig. 3. Quarter wavelength feed [13].

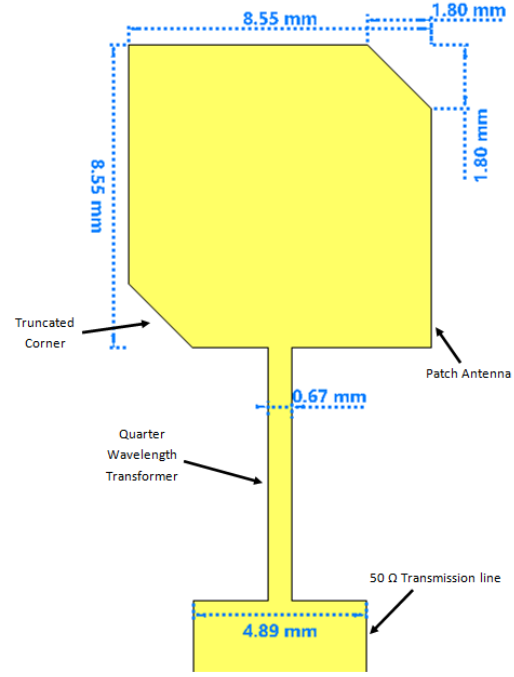


Fig. 4. Finalised element design.

The quarter wavelength feed was selected as it provides the most simplistic approach with minimal drawbacks. A coaxial feed cannot be easily extended to an array, and a resonant frequency shift is introduced by the inset feed.

The input impedance of the patch element, R_{in} , is required to calculate the quarter wavelength transformer impedance value. This is found using [5]

$$R_{in} = 90 \frac{\epsilon_r^2}{\epsilon_r - 1} \left(\frac{L}{W} \right) \quad (7)$$

resulting in $R_{in} = 363 \Omega$. Using this value, a quarter wavelength feed with an impedance of $Z_{0T} = 134 \Omega$ was calculated.

D. Element Optimisation

The patch element was manually optimised iteratively in CST Studio. The dimensions of the patch were adjusted in an attempt to maximise gain, S_{11} reflection coefficient, and AR, all at the centre frequency of 10.475 GHz. These performance parameters were required to meet or exceed the benchmark described in Section II-D. The final dimensions and design of the patch element can be seen in Figure 4.

The final design achieved a gain of 8.638 dBi, an S_{11} of -19.17 dB, and an AR of 2.14 dB at the antenna's centre frequency. These results meet the benchmark stated in section II-D, meeting the requirements.

E. CubeSat Antenna Array Design

The optimised patch antenna is used in an array to enhance gain and enable beamforming. Given the small size of the optimised element, it can be duplicated easily to create an

array on the 10 cm \times 10 cm face of the CubeSat. The total number of elements was constrained to the CubeSat's 10 cm \times 10 cm face, with each element requiring a separation of $\geq \frac{\lambda}{2}$ to avoid mutual coupling [15]. Based on these constraints, the number of elements, N , was selected to be 16. Using $\lambda = 28.62$ mm at 10.475 GHz, a separation of 20 mm between each element was used.

An array factor was used to determine array performance. This takes the element and duplicates it a specified number of times using set spacing (20 mm in this case) in order to simulate an array. It was established that an array of 16 elements with 20 mm spacing could produce a boresight gain of 20 dBi.

Whilst the array factor allows for the characterisation of an array, it is idealised and does not consider any imperfections that a realistic feeding network would exhibit. Future work should investigate a complete feeding network for this array.

Each element of the array is fitted with a phase shifter to enable steering of the main lobe. The direction of the main lobe is defined using spherical coordinates, with the elevation angle, θ , being referenced to the array's boresight, and the azimuth angle, ϕ , that rotates the beam around the plane perpendicular to the array's boresight. The progressive phase shifts required to achieve certain pointing angles can be found using [5]

$$\beta_x = -\frac{2\pi}{\lambda}d_x \sin(\theta) \cos(\phi) \quad (8)$$

$$\beta_y = -\frac{2\pi}{\lambda}d_y \sin(\theta) \sin(\phi) \quad (9)$$

where β_x and β_y are the required progressive phase shifts, and d_x and d_y are the spacing between the elements.

A constellation of finite pointing angles must be used to simulate a realistic system. The constellation's elevation angle is between $0^\circ \leq \theta \leq 90^\circ$ with a resolution of 5° . Its azimuth angle is between $0^\circ \leq \phi < 360^\circ$ with a resolution of 45° . Using (8) and (9), the required phase shifts were input into CST Studio to simulate the gain and beamwidth at these pointing angles. The gain of the main lobe is inversely proportional to the elevation angle due to side lobes becoming more predominant. Angles that reduced the main lobe's gain by > 3 dB were not included in the constellation. Angles that met the constraint were stored, along with their corresponding gain and beamwidths. These values were then used to form a constellation of usable pointing angles. The resulting constellation can be seen mapped onto a polar plot in Figure 5

F. Ground Station Antenna Array Design

The ground station is to be constructed using multiples of the CubeSat's antenna array. A set of these arrays operating in parallel ensures the ground station's achievable pointing angles match the constellation in Figure 5. Four copies of the original 16-element array will be used for the ground station. The four arrays work in parallel to increase the gain of the main lobe, without reducing the beamwidth that typically occurs with large arrays. The resulting increase in area provides a linear increase in gain. An increase by a factor of four results in a gain of 26 dBi.

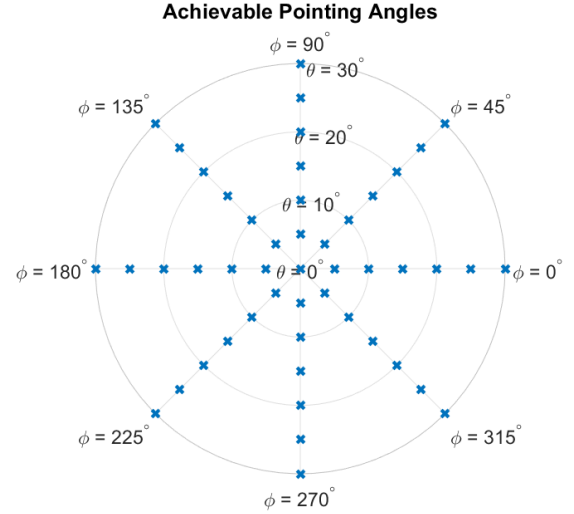


Fig. 5. Achievable pointing angles of the CubeSat's array.

IV. CHANNEL MODEL

A. Overview

The medium that the signals travel through is known as the communications channel. A channel model is a mathematical description of how signals are affected as they pass through this medium. It is crucial to understand how this medium impacts signals as it can cause significant degradation, which leads to errors being made by the system and therefore a high BER. A high BER restricts how much data can be transferred on the downlink, which thus limits the entire mission.

The received power of a signal at distance, d , is found using [9]

$$P_{rx}(d) = \frac{P_{tx}G_U G_D}{L_T(d)} \quad (10)$$

where G_U and G_D are the gain of the uplink (ground station) antenna and downlink (CubeSat) antenna respectively, and L_T is the total signal attenuation. L_T will now be broken down and modelled in the following sections.

B. Atmospheric Attenuation

1) *Overview*: Signals transmitted to and from a satellite must pass through Earth's atmosphere. As they pass through the atmosphere they undergo scattering and attenuation which heavily degrades the signal and results in errors being made by the demodulator. The atmosphere has a significant impact on signals at frequencies above 10 GHz as the wavelengths become small enough for degrading interactions with water droplets [9]. The troposphere, which extends from the ground up to an altitude of 15 km, is the predominant cause of attenuation due to precipitation and fog occurring in this region [9], [16].

2) *Rain Attenuation*: Rain attenuation is the predominant cause of attenuation of signals operating above 10 GHz [9]. The intensity of precipitation is measured by the rainfall rate, R_p (mm/h), where p is the annual percentage of time this

rainfall rate is exceeded. Attenuation due to precipitation, A_{RAIN} , can be found using

$$A_{\text{RAIN}} = \gamma_{\text{R}} L_e \quad (11)$$

where γ_{R} (dB/km) is the specific attenuation, and L_e (km) is the effective path length that the wave travels in the rain. The specific attenuation is a measure of how much a signal is attenuated per unit length for a given operating frequency and rainfall rate. It provides a value of attenuation per unit length that is exceeded $p\%$ of the time per year. It can be found using

$$\gamma_{\text{R}} = k R^\alpha \quad (12)$$

where

$$k = \frac{k_{\text{H}} + k_{\text{V}} + (k_{\text{H}} - k_{\text{V}}) \cos^2(E) \cos(2\tau)}{2} \quad (13)$$

$$\alpha = \frac{k_{\text{H}}\alpha_{\text{H}} + k_{\text{V}}\alpha_{\text{V}} + (k_{\text{H}}\alpha_{\text{H}} - k_{\text{V}}\alpha_{\text{V}}) \cos^2(E) \cos(2\tau)}{2k} \quad (14)$$

where k is the frequency-dependent coefficient that accounts for specific attenuation for precipitation, with k_{H} and k_{V} accounting for horizontal and vertical polarisation aspects respectively. α is the frequency-dependent coefficient that accounts for specific attenuation due to the atmosphere, with α_{H} and α_{V} accounting for horizontal and vertical polarisation aspects respectively. The values for k_{H} , k_{V} , α_{H} , and α_{V} can be found in [17]. These values were identified to be $k_{\text{H}} = 0.012$, $k_{\text{V}} = 0.010$, $\alpha_{\text{H}} = 1.261$, and $\alpha_{\text{V}} = 1.248$. Using (13) and (14), and using $f = 10.475$ GHz, $\tau = 45^\circ$ (polarisation tilt angle for circular polarisation), and $E = 10^\circ$, the coefficients were calculated, resulting in $k = 0.011$ and $\alpha = 1.255$. International Telecommunication Union (ITU) provides data on rainfall rates for New Zealand, which shows that the rainfall rate exceeded 0.01% of the time in New Zealand is $R_{0.01} = 25$ mm/h [9]. Finally, using (12) $\gamma_{0.01} = 0.625$ dB/km.

L_e for 0.01% of the time in (11) is found through

$$L_e = L_{\text{R}} \nu_{0.01} \quad (15)$$

where L_{R} is the slant-path length and is found using

$$L_{\text{R}} = \begin{cases} L_{\text{G}} r_{0.01} & \text{for } \zeta > E \\ (h_{\text{R}} - h_{\text{S}}) / \sin E & \text{otherwise} \end{cases} \quad (16)$$

where h_{R} (km) and h_{S} (km) are the effective height of the rain and the height of the Earth station above mean sea level respectively, and ζ is the effective elevation. h_{R} is found using

$$h_{\text{R}}(\text{km}) = h_0 + 0.36 \quad (17)$$

where h_0 is the mean 0°C isotherm height above mean sea level and is found to be 1 km in New Zealand through [9]. Thus, using (17) $h_{\text{R}} = 1.36$ km. The ground station is to be situated at VUW, thus the ground station's height above mean sea level is $h_{\text{S}} = 0.1$ km. ζ is found through [9]

$$\zeta = \arctan\left(\frac{h_{\text{R}} - h_{\text{S}}}{L_{\text{G}} r_{0.01}}\right) \quad (18)$$

where L_{G} and $r_{0.01}$ are the horizontal projection of slant-path length and the horizontal reduction factor respectively. L_{G} is found to be 7.15 km using [9, eq 5.45.4], and $r_{0.01}$ is found to be 0.885 using [9, eq 5.45.6], resulting in $\zeta = 11.268$ through (18). Using the minimum elevation angle of $E = 10^\circ$, it can be concluded that $\zeta > E$. Thus, using (16) $L_{\text{R}} = 6.421$ km.

Lastly, the vertical adjustment factor, $\nu_{0.01}$, is found using [9]

$$\nu_{0.01} = \left[1 + \sqrt{\sin E} \left(31 \left(1 - e^{-(E/(1+\chi))} \right) \frac{\sqrt{L_{\text{R}} \gamma_{\text{R}}}}{f^2} - 0.45 \right) \right]^{-1} \quad (19)$$

where the value of χ is based on the ground station's latitude and is found to be $\chi = 0$ [9, eq 5.45.7]. $\nu_{0.01}$ is thus calculated to be 1.273. In summary

TABLE I
TABLE OF RAIN ATTENUATION PARAMETERS

Symbol	Parameter	Value
k_{H}	Precipitation coefficient (horizontal)	0.012
k_{V}	Precipitation coefficient (vertical)	0.010
α_{H}	Atmosphere coefficient (horizontal)	1.261
α_{V}	Atmosphere coefficient (vertical)	1.248
f	Operating frequency	10.475 GHz
τ	Polarisation tilt angle	45°
E	Elevation angle	10°
$R_{0.01}$	Rainfall intensity 0.01%	25 mm/h
$\gamma_{0.01}$	Specific attenuation 0.01%	0.625 dB/km
h_0	Mean 0°C above height sea level	1 km
h_{R}	Effective height of rain	1.36 km
h_{S}	Height ground station above sea level	0.1 km
L_{G}	Horizontal projection of slant-path	7.15 km
ζ	Effective elevation	11.268 km
$r_{0.01}$	Horizontal reduction factor	0.885
L_{R}	Slant-path length	6.421 km
$\nu_{0.01}$	Vertical adjustment factor	1.273

Substituting these values into (11) results in an attenuation value of $A_{\text{RAIN}} = 5.11$ dB. This value is the level of attenuation that will be exceeded 0.01% of the time per year, meaning the system will perform better 99.9% of the time. This is used to understand the link budget in the worst-case scenario to ensure the system remains operational despite intense precipitation.

3) *Fog Attenuation*: Signals propagating through Earth's atmosphere are subject to attenuation due to the formation of fog or clouds. This effect is of concern for systems operating within a frequency range of 1 to 30 GHz [9]. The specific attenuation due to fog or clouds can be found through

$$\gamma_f = KM \quad (20)$$

where $K = 1.2 \times 10^{-3} f^{1.9}$ is the specific attenuation coefficient, and M is the liquid water density in gm^{-3} [9]. A typical value of the liquid water density in thick clouds is $M = 0.5 gm^{-3}$, resulting in $\gamma_f = 0.052$ dB/km [9]. This attenuation can then be multiplied by the path length, R (km), to find the total attenuation due to fog. The path length used in this equation is the depth of the clouds, which varies considerably on any given day. Thus, the worst-case value of

2 km is used [18]. This path length results in an attenuation due to fog of 0.104 dB using

$$L_f = R\gamma_f \quad (21)$$

This value is insignificant compared to the attenuation to rain, however, it is observed for a greater percentage of the time, that being 1% [9]. It should therefore be considered as a part of this channel model.

C. Path Loss

Free space path loss is the predominant cause of attenuation in this channel model. It is the loss of power as the signal is radiated through free space. The value of the path loss can be found using

$$L_{FS} = \left(\frac{4\pi Rf}{c} \right)^2 \quad (22)$$

where R is the distance travelled by the signal, f is the frequency, and c is the speed of light.

D. Total Attenuation

The effects of attenuation are combined into the single value L_T which can be used in (10). L_T can be found using the following equation

$$L_T = A_{RAIN}L_fL_{FS} \quad (23)$$

E. Noise and Interference

Noise consists of unwanted variations in the carrier signal within the system's operational bandwidth. It adds noise power to the carrier signal, which causes it to vary from its intended shape. This causes fluctuations in the received signal power and shape, resulting in demodulation errors occurring. Noise can originate within the system from components of the receiving circuit, or from external natural sources of radiation, whose emissions are within the reception of the receiving antenna system. This can originate from galactic noise, atmospheric absorption, and thermal radiation from the Earth; signals originating from other transmitters operating at the same frequency will contribute to the received noise as interference.

Noise in communications systems is modelled as an effective temperature, T , which represents the thermodynamic temperature of resistance that would produce an equivalent value of noise as the considered source [9].

The effective temperature of the antenna, T_A , is a measure of the total noise it receives from natural sources, such as the sky, T_{SKY} , which is due to the cosmic background and noise due to the atmosphere. T_{SKY} varies significantly with frequency, with frequencies between 1 to 10 GHz showing the lowest value at around 10 K [13]. Systems operating in lower frequency bands, such as ultra high frequency (UHF), are more susceptible to galactic noise, with this value dropping off as the frequency approaches 1 GHz. The temperature due to atmospheric noise increases as the frequency increases from

1 GHz, with the impact peaking at 23 GHz due to interactions with water molecules, and again at 60 GHz due to interactions with oxygen molecules [13]. As the proposed system operates at 10.475 GHz the effect of cosmic and atmospheric noise is less significant. T_{SKY} varies with elevation angle, as such, the worst case of 10° is to be used. Provided in [9] is data on T_{SKY} as a function of frequency and elevation angle for clear sky conditions. At an elevation of 10° and a frequency of 10.475 GHz the value for T_{SKY} is 18 K.

The effective temperature of the antenna increases in the presence of precipitation [9]. As discussed in Section IV-B2, the water molecules present due to precipitation interact with the signals due to their small wavelength and create an absorbent medium. As a result, this medium becomes emissive and adds to antenna noise. This noise is factored into the antenna temperature equation through the use of A_{RAIN} as seen in (24). The mean thermodynamic temperature of these atmospheric formations is denoted T_m , and a value of 275 K can be assumed [9].

The Earth radiates thermal noise due to blackbody radiation, which results in it contributing to the value of T_A with its typical ambient temperature of 290 K [13]. However, as the proposed system utilises a directional antenna, this value is not entirely captured by the system [9]. Radiation from the ground is primarily captured by the antenna's side lobes due to its directional properties. At low elevation angles, it is possible for noise to be captured by the main lobe which causes increased noise due to the higher gain [9]. As the system communicates at elevation angles between $10^\circ < E < 180^\circ$, the noise contributed by the ground is low. It is stated in [9] that the effective noise temperature of the ground as a first approximation can be taken 10 K for elevation angles $10^\circ < E < 90^\circ$. The noise temperature for the ground is therefore taken as 10 K for this project. T_A is found using

$$T_A = \frac{T_{SKY}}{A_{RAIN}} + T_m \left(1 - \frac{1}{A_{RAIN}} \right) + T_{GROUND} \quad (24)$$

where T_m is the mean thermodynamic temperature and T_{GROUND} is the effective temperature of the ground. Using the values of $T_{SKY} = 18$ K, $T_{GROUND} = 10$ K, and $A_{RAIN} = 5.11$ dB in (24), the value T_A was calculated to be 207.61 K.

The noise power spectral density, N_0 , describes the amount of noise present per unit bandwidth (or per Hz). It can be found using

$$N_0 = kT \quad (25)$$

where k is the Boltzmann's constant. Using $T = 207.61$ K, the noise power spectral density was calculated to be $N_0 = 2.9 \times 10^{-21}$ W/Hz = -205.4 dBW/Hz.

This value is multiplied by the total bandwidth used by the system to find the total noise power, N , present in the system. That is

$$N = N_0B \quad (26)$$

where B is the bandwidth of the system. Thus, as the bandwidth is increased the amount of noise captured by the

antenna increases. The carrier-to-noise ratio, $\frac{C}{N}$, can then be found using this value. This is a commonly used measurement to identify the performance of a communications system. It measures the strength of the received signal compared to the received noise power. If noise power far exceeds signal power then system performance will be extremely limited.

The carrier-to-noise value considers the received power and noise ratio before the signal is processed and demodulated. This means that it does not take into account noise due to internal sources, such as processing circuitry. This is in contrast to the signal-to-noise ratio that is commonly used in the analysis of terrestrial systems. The carrier-to-noise ratio was used in this research in an effort to determine the effect that the channel has on the transmitted signal. The channel is the limitation of this communications project. It cannot be avoided and cannot be improved, thus, it was of relevance to solely investigate $\frac{C}{N}$. The electronics that contribute to noise during processing within the CubeSat can be improved with added expenditure, thus, it is not a crucial aspect of this project.

Random fluctuations of noise in the received signal lead to symbols being incorrectly demodulated. Additive White Gaussian Noise (AWGN) is a popular model of random noise that is used to simulate real-world noise. It follows a Gaussian distribution with a mean of zero and a variance of $\sqrt{\frac{N}{2}}$.

F. Channel Capacity

The fixed values of the channel model are now summarised in Table II. The theoretical capacity per Hz of the channel can be calculated using (27).

TABLE II
TABLE OF FIXED CHANNEL MODEL VALUES

Symbol	Parameter	Value
A_{RAIN}	Rain attenuation	5.11 dB
T_{SKY}	Effective temperature of the sky	18 K
T_{GROUND}	Effective temperature of Earth	10 K
T_{A}	Effective temperature of the antenna	512.86 K
N_0	Noise power spectral density	-201.5 dB

$$C = \log_2(1 + P_{\text{rx}}/N_0) \quad (27)$$

where P_{rx} is found using (10).

Figure 6 shows the theoretical capacity as a function of altitude; it demonstrates the expected drop in performance as the system approaches its peak altitude of 38,786 km, however, even at such extreme altitudes the theoretical capacity shows the requirements can be met (in theory) given the abundant bandwidth. Though achieving this theoretical capacity is not practical, it does provide a benchmark for the system.

V. MODULATION

A. Spectrum Shaping

Spectrum shaping in a wireless communications system is essential for restricting signals in both the time and frequency domain to comply with restrictions described in Section III-A. This is typically achieved through a pulse shaping function,

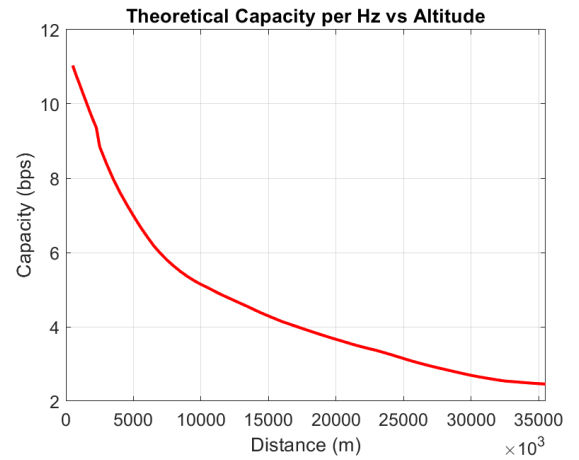


Fig. 6. Theoretical capacity as a function of altitude.

which determines the spectral characteristics of transmitted signals. However, utilising these pulse shaping functions introduces inter-symbol interference (ISI) which can significantly degrade performance [9]. The Nyquist bandwidth constraint states that the minimum bandwidth, B , required for a symbol rate of R_s without ISI is $\frac{R_s}{2}$ [19]. The minimum bandwidth requirement described can be achieved through the use of a rectangular bandpass filter, however, this is not used in practice as a filter with such sharp edges is not attainable. Furthermore, a rectangular filter corresponds to a very slowly decaying symbol in the time domain. This means the symbol would exhibit tails with large amplitudes which can therefore interfere with adjacent symbols if timing errors occur in the receiving circuitry [9]. Conversely, if the implemented filter exhibits a smoother cut-off then the tails of the time domain symbol decay at a faster rate, minimising errors due to mistimed sampling.

A commonly used pulse shape function is the raised-cosine pulse, which has the bandwidth-to-symbol rate relationship described by

$$B = \frac{1}{2}(1 + r)R_s \quad (28)$$

where r is the roll-off factor of the pulse. This factor describes how “relaxed” the pulse is in the frequency domain. When $r = 1$, the bandwidth is maximised at $B = R_s$; when $r = 0$, the bandwidth is minimised and sets to the bandwidth to the Nyquist rate of $B = \frac{R_s}{2}$. The use of the raised-cosine in this project allows bandwidth requirements to be identified. Using a roll-off factor of $r = 0$ leads to problematic demodulation due to the required sampling precision described above. Therefore, as the system is not limited in terms of available bandwidth, this project will use a raised-cosine with a roll-off factor of $r = 1$.

B. FSK

Frequency shift keying (FSK) is a commonly used modulation scheme in satellite communications. In FSK each symbol is represented by a carrier with frequency shifts depending on

whether a 1 or a 0 is being sent. For the case of BFSK, the basis pulses are

$$\phi_{BP,1} = \sqrt{2/T_B} \cos(2\pi f_c t + 2\pi f_{\text{mod}} t) \quad (29)$$

$$\phi_{BP,0} = \sqrt{2/T_B} \cos(2\pi f_c t - 2\pi f_{\text{mod}} t) \quad (30)$$

where f_{mod} is the change in frequency denoting a 1 or a 0 [4].

FSK suffers from abrupt changes at symbol transitions which results in a non-constant envelope [4]. Satellite links undergo significant fluctuations in amplitude due to atmospheric attenuation (see Section IV). Signals with non-constant envelopes are more susceptible to distortion in these types of channels as their variations in amplitude can become amplified by attenuation events, such as heavy precipitation [20].

C. PSK

Phase-shift keying is a modulation scheme that characterises its constellation points as a set of phase-shifted symbols. The simplest form of this is BPSK, where the carrier phase is shifted by $\pm\pi/2$. This results in the outputs Ae^{j0} or $Ae^{j\pi}$, denoting a 0 or a 1, where A is the amplitude of the signal. This modulation scheme can be interpreted as phase modulation, or as binary pulse amplitude modulation (PAM) because the two described positions on the complex plane simplify to A or $-A$, which is equivalent to binary PAM modulation. BPSK is to be utilised in this simulation as it is well-suited to satellite communications due to its signal exhibiting a constant envelope [9].

VI. SIMULATION

A. Keplerian Orbits

Keplerian orbits are characterised by elements that define the path and position that an orbiting body takes. The position vector of an orbiting body at time t can be found using the six Keplerian elements. This is given by [21]

$$\vec{r}(t) = \vec{r}(t; a, e, i, \Omega, \omega, \nu) \quad (31)$$

where a is the semi-major axis, e is eccentricity, i is inclination, Ω is the right ascension of ascending node, ω is the argument of perigee, and ν is the true anomaly. Figure 7 provides a visualisation of these elements.

The elements of the Keplerian orbit were selected to maximise coverage over New Zealand. The elements were optimised through Matlab's Satellite Communication Toolbox (SCT), with the results being shown in the table below

TABLE III
SELECTED KEPLERIAN ELEMENT VALUES

Element	Value
a	6871 to 42164 km
e	0
i	43°
Ω	0°
ω	-45°
ν	-135°

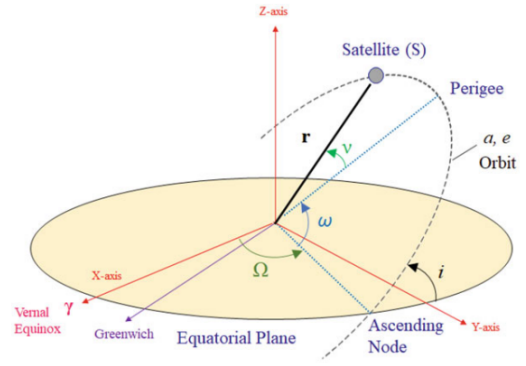


Fig. 7. Keplerian Orbital Parameters [9].

B. Orbital Characterisation

The CubeSat's relative position to New Zealand during its pass-over is constantly changing. Each revolution around Earth results in the CubeSat passing with a different elevation and azimuth angle. The CubeSat's beam must constantly adapt to ensure a link is maintained. As discussed in Section III-E, the CubeSat incorporates a phased array that allows the antenna array to steer its beam toward the ground station. Angling the beam off its boresight reduces the gain, as such, the gain of the main lobe will vary as it is being steered. This must be considered to ensure accurate results.

C. Orbital Geometry Analysis

Matlab's SCT provides elevation and azimuth angles of the satellite during its entire orbit. The angles of the CubeSat in orbit at varying semi-major axes were collected. Samples of each angle were taken every 10 seconds from the bottom of LEO to the top of MEO as these orbits are dynamic and have dramatic changes in position. From the top of MEO to GEO, the position is sampled every 30 seconds as these orbits are predominantly static.

To determine which of these angles corresponded to a feasible communications link each data point in time was compared to a table of possible communication time intervals that were also found through the SCT. The time intervals were identified with a ground station elevation angle constraint of $10^\circ < \theta < 170^\circ$. This means that the satellite was able to communicate with the ground station when it met these constraints during its orbit.

The law of sines was used to find the distance, d , to the ground station at each sampled position in orbit. The satellite in orbit creates a triangle as shown in Figure 8.

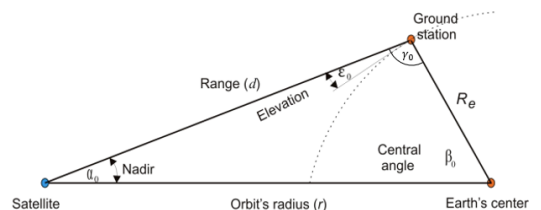


Fig. 8. Geometry of the satellite's orbit [22].

As the angle, α_0 , from the antenna boresight (angled directly at the centre of the Earth) is known, the law of sines can be employed to find γ_0 using

$$\gamma_0 = 180^\circ - \arcsin\left(\frac{r_S \times \sin(\alpha_0)}{r_E}\right) \quad (32)$$

where r_E and r_S are the radius of the Earth and the semi-major axis of the orbit respectively. The law of sines does not always uniquely determine the solution as it is possible that multiple triangles can be formed using the input data. In this case, the law of sines was providing a solution to a triangle with a small value for γ_0 . As the elevation angle, ϵ_0 , cannot be less than 10° , γ_0 cannot be less than 100° . Therefore, the inverse angle from the law of sines was found by subtracting the angle from 180° .

Knowing γ_0 allows the third angle, β_0 , to be identified using the triangle angle sum theorem. Finally, the distance, d , from the satellite to the ground station can be identified using the Law of Cosines using the following equation

$$d = \sqrt{r_E^2 + r_S^2 - 2r_E r_S \times \cos(\beta_0)} \quad (33)$$

These calculations were carried out for the constellation angles (detailed in Section III-E), and the sampled angles that overlapped with the communication intervals, which resulted in an array of angles and distances. The simulated angles must be mapped to the constellation of finite angles that the system can achieve. To determine the closest constellation point to the simulated point the Euclidean distance from the simulated point to each constellation point is found. The constellation point corresponding to the shortest Euclidean distance is then selected.

In some cases, the constellation of pointing angles will not have enough spatial resolution to provide coverage for a link to the ground station. In these situations communication is not possible and the data point is disregarded. To determine if the selected constellation point can provide coverage, the beamwidth and distance to the ground station are used to calculate the radius of the beam on the Earth's surface. The radius of the beam on the surface is compared to the Euclidean distance between the ground station and the centre of the beam. If the ground station lies within that radius then communication is possible.

D. Simulated Data Link

The data extracted in Section VI-C can then be used in a simulated data transfer to identify the potential performance of the system. The distance and gain of each sample are fed into a function that simulates the transmission of a vector of 1000 bits, denoted \vec{s} , at a specified data rate, R_s , and transmit power, P_{tx} . Based on these values the energy of each transmitted symbol can be found using

$$E_{stx} = \frac{P_{tx}}{R_s} \quad (34)$$

This value determines where the symbols sit on the BPSK constellation plot. As described in Section V-C, the system

will be using BPSK as its modulation scheme, thus, the two possible symbols will be $-\sqrt{E_{stx}}$ and $\sqrt{E_{stx}}$.

The energy of the transmitted symbol will be heavily attenuated as it passes through the channel model described in Section IV. The received power of the system can be calculated using (10), which leads to the received energy, E_{srx} , by using P_{rx} in (34). The energies in \vec{s} can then be converted by dividing the received energies by the transmitted energies, that is, $\vec{r} = \frac{\sqrt{E_{srx}}}{\sqrt{E_{stx}}} \vec{s} = \sqrt{E_{srx}} \vec{s}$.

As described in Section IV-E, the noise present in the system is the product of the noise power spectral density, N_0 , and the bandwidth of the system, B . It is therefore necessary to minimise the bandwidth to reduce noise. Section V-A detailed the use of a relaxed raised cosine pulse shape, which results in the required bandwidth for the system being equal to its data rate. Thus, the simulated bandwidth, B , was set equal to the specified data rate for each simulation. This reduces the received noise power, which thus reduces the variance of the AWGN distribution. Resultingly, AWGN with a mean of 0 and a variance of $\sqrt{N/2}$, denoted \vec{n} , is combined with \vec{s} to simulate real-world random noise. This results in the received vector $\vec{r} = \sqrt{E_{srx}} \vec{s} + \vec{n}$. The closest constellation point of each element in \vec{r} is found, which is then compared with the transmitted vector. Elements that match are taken as a successful data transfer, and those that do not match are considered errors. The ratio of errors to the number of transmitted bits is used to calculate the BER. The collected data in Section VI-C is a sample of either 10 seconds for LEO and MEO, and 30 seconds for GEO; data transfer must be simulated for the total sample time. The total successful data transfer for each sample is therefore $DT = \frac{DR_s}{1000} \times 30$, where D is the total number of successful bits from \vec{r} . The total errors for each sample is therefore $ET = \frac{ER_s}{1000} \times 30$, where E is the total number of errors from \vec{r} . These values allow the BER per altitude to be calculated through

$$\text{BER} = \frac{ET}{ET + DT} \quad (35)$$

E. Simulation Results and Discussion

The requirements set out in Section I state that the mission aims to measure Earth's magnetic field with a resolution of one sample per km in orbit. Each sample is to consist of four scalar quantities, each quantised to 16 bits. To quantify the throughput required, the total data collected per orbit can be calculated. At the lower end of LEO at 500 km, the circumference of the orbit is $C = 2\pi r = 43172$ km, where $r = 6371 + 500$ km is the semi-major axis of the orbit. Thus, the number of samples required at an altitude of 500 km is 43172 per orbit, which allows the total data per orbit to be calculated as $D = 43172 \times 16 \times 4 = 2.76$ Mb per orbit.

At LEO the link time per orbit varies significantly, with some revolutions resulting in communication only being available for a matter of seconds. A simulation that tracks link times over three days was used to gain a greater understanding of the feasibility of transmitting the required payload. The amount of data collected over three days is proportional to the number of revolutions completed within that time. The number

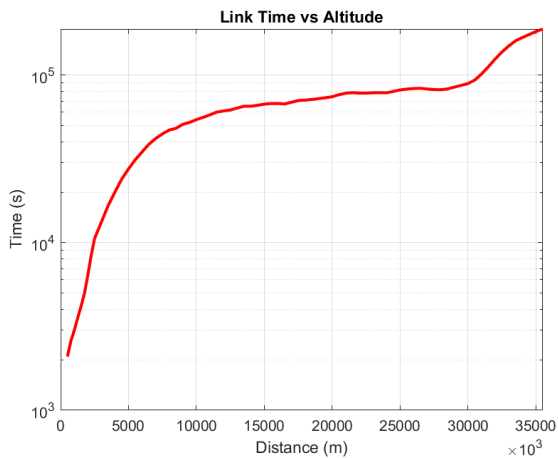


Fig. 9. Available link time across three days.

of revolutions can be calculated by dividing three days by the orbital period, which can be calculated using [23]

$$T = 2\pi\sqrt{\frac{(R_E + h)^3}{G \times M_E}} \quad (36)$$

where R_E is the radius of the Earth, h is the altitude of the orbit, G is the gravitational constant of Earth, and M_E is the mass of the Earth. The total data collected over three days is thus $D_{\text{tot}} = D \times N$, where N is the calculated number of revolutions. The required data rate is inversely proportional to the link time, which can be found using the orbital data acquired in Section VI-C. It can be seen that the number of orbital samples during available link times was 68 at an altitude of 500 km, thus multiplying this by the sample period of 10 seconds results in a total link time across three days of only 680 seconds for an altitude of 500 km. The total link time across three days for altitudes ranging from LEO to GEO can be seen in Figure 9.

The required data rate can be found by dividing the total data by the link time. Figure 10 details the required data rates as a function of altitude, which shows very high data rates at lower altitudes. This is due to the very small link times with a large number of revolutions. The required data rate falls steeply with altitude due to increased link times. It is thus important to understand the performance of the system with these orbital constraints.

To quantify the performance of the system the simulation was run at varying bit rates with a constant transmit power of 1 W. Figure 11 shows the BER vs altitude for four bit rates. Whilst the performance at low altitudes is sufficient to transmit data with minimal errors, it cannot achieve the unrealistic requirement of approximately 10^5 bps shown in Figure 10 using only 1 W of power. Furthermore, the required bit rate at greater altitudes cannot be met due to the BER approaching 0.5 (completely random). An increase in transmitting power or a decrease in the sample rate must be considered to better utilise the communications system.

Figure 12 shows the simulation of the required bit rates for 5000 km, 20000 km, and 35786 km with a transmit power of 5 W. It demonstrates that a small increase in transmit

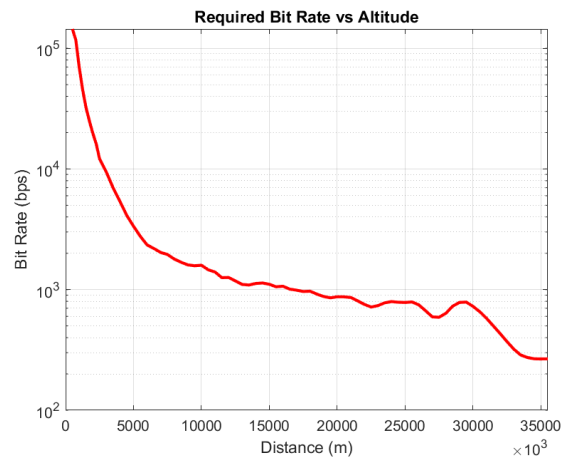


Fig. 10. Required bit rate to transmit data collected over three days.

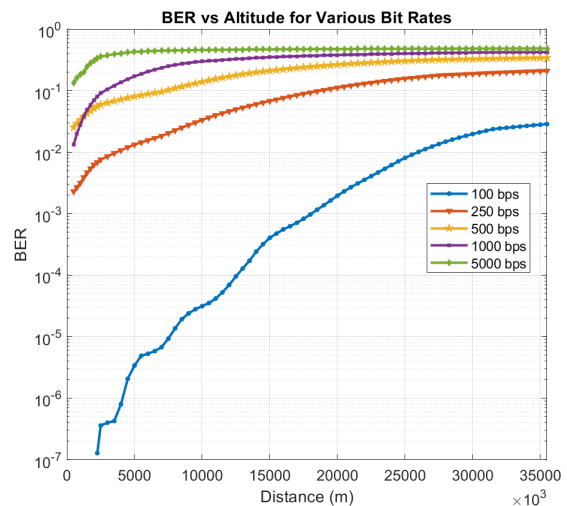


Fig. 11. Simulation of data transfer at 1 W for varying data rates.

power significantly decreases the system's BER, thus enabling the system to operate near the required bit rates set out in Figure 10. The increased power reduces the impact noise has during demodulation, reducing the probability of an error. The increase from 1 to 5 W results in a BER reduction of 1 order of magnitude for 270 bps at 35786 km, which becomes low enough to utilise ARQ. FEC codes are required for 900 bps at 20000 km, and 3500 bps at 5000 km which experienced BERs of around 0.2. These techniques are discussed further in Section VII. Bit rates at altitudes less than 5000 km were not investigated further due to their unfeasible requirements. A lower sample rate or long-term storage with transmission occurring at altitudes with increased link time must be considered.

VII. CHANNEL CODING

A. Overview

Channel coding is an area of communications that involves the detection and correction of errors. ARQ and FEC are two commonly used methods for error correcting. ARQ is the simplest approach, which is to have the message repeated if

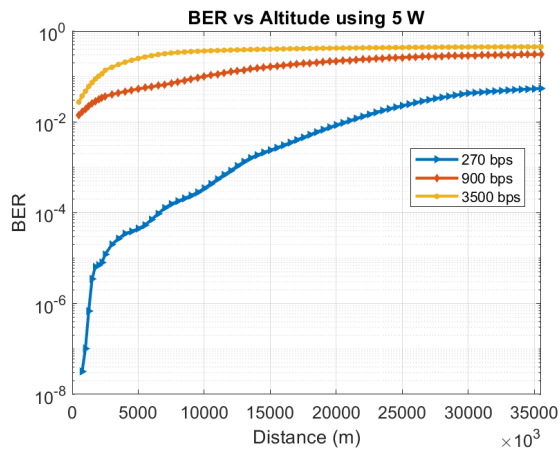


Fig. 12. Simulation of data transfer at 3500 bps (5000 km), 900 bps (20000 km), and 270 bps (35786 km) using 5 W.

an error is detected. This method, along with being incredibly simple to implement, does not require any overhead, which means when in low BER systems it is more bandwidth efficient than FEC. However, in systems where errors are likely to occur this method performs poorly. Instead, FEC becomes the preferred method due to its ability to automatically correct errors without requiring the entire message to be resent. FEC encodes the message with redundancy prior to it being sent which allows the receiver to deal with any errors. This method has seen the performance of systems approach Shannon's capacity (see Section IV-F) [4].

The BERs shown in Figure 11 will result in a communications system with significant errors when using the required bit rates with 1 W of power. Whilst mathematically the amount of data received successfully is enough to fulfil the requirements outlined in Section I, in a practical system that utilises data packets, it will be statistically very rare to receive a complete packet without errors. A system that does not utilise FEC will rely purely on the simplistic ARQ technique. Whilst this technique is effective in systems with a low probability of error, it works poorly in systems with high error rates and results in wasted link time. The expected number of repeats required to receive m bits consecutively can be found using [24]

$$E[N] = \frac{1 - p^m}{qp^m} \quad (37)$$

where N is the number of repeats required to achieve m consecutive successes, p is the probability of success, and q is the probability of failure. At GEO and using 1 W of transmit power with a bit rate of 270 bps, the BER was found to be $q = 0.22$, thus $p = 1 - 0.22 = 0.78$. Using (37) we find that the expected number of attempts to receive a typical packet size of 10 bits is about 50. Dividing this value by the packet size indicates the number of ARQs required, which in this case is 5. This is clearly an inefficient use of the system's link time and provides clear justification for the use of FEC. This can then be used in conjunction with ARQ to provide a reliable communications link.

B. Turbo Codes

Turbo coding is a convolutional coding scheme that utilises a parallel structure. Several streams are fed into the encoder in parallel, with each stream interleaved by a pseudorandom interleaver. Interleaving spreads and scrambles the input data which helps spread burst errors that are often attributed to significant weather events [25]. The individual streams are combined into a single output that includes the original data sequence and added redundancy.

The decoder works iteratively to identify the original sequence. The data stream is passed through multiple stages, with each stage attempting to decode the original and assigning a reliability value to each bit. This is passed through each state until the decoder is able to confidently determine the original sequence [4]. This decoding method is computationally expensive, requiring around 400-800 operations per information bit [4], rendering its use on the CubeSat unfeasible due to its limited resources. Instead, it is proposed that the downlink incorporate turbo codes as this includes a majority of the data transfer and only requires decoding at the ground station which is not resource-constrained. Errors occurring on the uplink can be circumvented with ARQ and a boosted transmit power.

The code rate, R_c , describes the ratio of information bits to redundancy bits. It is a measure of how efficient the coding method is and dictates its error-correcting capability. It is found using

$$R_c = \frac{n}{n + r} \quad (38)$$

where n and r are the information and redundancy bits respectively.

It is stated in [26] that with a $1/2$ code rate a BER of 10^{-5} could be achieved using quadrature phase shift keying (QPSK) with carrier-to-noise ratio (CNR) of 4.4 dB. This project showed a BER of 0.22 with a CNR of 6.2 dB at the project's peak altitude, a transmit power of 1 W, and using BPSK. In the absence of turbo coding gain at this higher CNR and less dense modulation scheme, the BER of 10^{-5} will be used as an indicator. Using (37) the expected number of attempts with this BER is 1. This shows that through the use of turbo coding the required bit rate at GEO could be met.

VIII. CONCLUSION

This project has presented a design framework for an end-to-end CubeSat communications model that can be utilised in advanced CubeSat missions. The results demonstrated the significant impact that available link time has on achieving mission requirements. Simulations of the model at varying transmit powers and bit rates allow mission planners to determine payload capabilities in orbits ranging from LEO to GEO. Turbo codes were demonstrated to play a vital role in enhancing the capabilities of communications systems onboard low-power satellites. The feasibility of such communications systems being deployed on CubeSats operating across a range of altitudes is shown through these results. This drives ambitious missions involving advanced orbit manoeuvres by miniaturised satellites.

IX. FUTURE WORK

The aim of this project was to provide mission planners with an understanding of achievable throughput. This included identifying the performance of the system using a channel model that incorporated the most significant attenuators. Further work is required to refine the model.

The developed channel model provides worst-case effects on propagating signals. Whilst this provided a baseline, further research should investigate stochastic atmospheric models to identify any improvements in performance.

Satellites operating in LEO have high velocities relative to observers on Earth. A Doppler shift is introduced in signals being transmitted to Earth from these orbits. This will result in signal phase shifts that can generate phase-shift keying (PSK) demodulation errors. The effect on performance should be investigated, and techniques to correct these shifts should be evaluated.

High frequency circuitry used in communications systems introduces noise to the system. This is known as processing noise and can degrade system performance. The CNR was used in this model as this provides insight into the effects of the channel. The signal-to-noise ratio (SNR) accounts for both external and internal noise. Internal noise originates from the processing circuitry. The impact of internal noise should be investigated and understood.

An array feeding network should be designed and modelled to identify any impact on performance. Furthermore, a set of this array should be simulated to investigate the performance of the ground station.

REFERENCES

- [1] Z. Jaeger-Letts, J. Glowacki, and C. Hollitt, "Mission design and analysis of an electric propulsion nanosatellite mission." 2022.
- [2] A. Witze, "The quest to conquer the space junk problem," *Nature*, vol. 561, no. 7721, pp. 24–26, 2018.
- [3] S. Abulgasem, F. Tubbal, R. Raad, P. I. Theoharis, S. Lu, and S. Iranmanesh, "Antenna designs for cubesats: A review," *IEEE Access*, vol. 9, pp. 45289–45324, 2021.
- [4] A. F. Molisch, *Wireless communications: from fundamentals to beyond 5G*. John Wiley & Sons, 2022.
- [5] C. A. Balanis, *Antenna Theory: Analysis and Design*. John Wiley & sons, 2016.
- [6] I. S. M. Hashim, A. Al-Hourani, S. W. Rowe, and J. R. Scott, "Adaptive x-band satellite antenna for internet-of-things (iot) over satellite applications," in *2019 13th International Conference on Signal Processing and Communication Systems (ICSPCS)*, pp. 1–7, IEEE, 2019.
- [7] S. Gao, Y. Rahmat-Samii, R. E. Hodges, and X.-X. Yang, "Advanced antennas for small satellites," *Proceedings of the IEEE*, vol. 106, no. 3, pp. 391–403, 2018.
- [8] NZART, "Nzart band plans @ONLINE." <https://www.nzart.org.nz/info/band-plan/>, 2023.
- [9] G. Maral, M. Bousquet, and Z. Sun, *Satellite communications systems: systems, techniques and technology*. John Wiley & Sons, 2020.
- [10] R. Mishra, "An overview of microstrip antenna," *HCTL Open International Journal of Technology Innovations and Research (IJTIR)*, vol. 21, no. 2, pp. 39–55, 2016.
- [11] S. X. Ta, V. D. Le, K. K. Nguyen, and C. Dao-Ngoc, "Planar circularly polarized x-band array antenna with low sidelobe and high aperture efficiency for small satellites," *International Journal of RF and Microwave Computer-Aided Engineering*, vol. 29, no. 11, p. e21914, 2019.
- [12] R. Waterhouse and R. Waterhouse, "Improving the efficiency of microstrip patch antennas," *Microstrip Patch Antennas: A Designer's Guide*, pp. 167–195, 2003.
- [13] C. E. Free and C. S. Aitchison, *RF and Microwave Circuit Design: Theory and Applications*. John Wiley & Sons, 2021.
- [14] T. Prabhu, S. C. Pandian, and E. Suganya, "Contact feeding techniques of rectangular microstrip patch antenna for 5 ghz wi-fi," in *2019 5th International conference on advanced computing & communication systems (ICACCS)*, pp. 1123–1127, IEEE, 2019.
- [15] D. A. Jiménez, A. Reyna, L. I. Balderas, and M. A. Panduro, "Design of 4 × 4 low-profile antenna array for cubesat applications," *Micromachines*, vol. 14, no. 1, p. 180, 2023.
- [16] S. Gong, D. Wei, X. Xue, and M. Y. Chen, "Study on the channel model and ber performance of single-polarization satellite-earth mimo communication systems at ka band," *IEEE Transactions on antennas and propagation*, vol. 62, no. 10, pp. 5282–5297, 2014.
- [17] I. R. P. Series, "Specific attenuation model for rain for use in prediction methods," *Rec. P. 838-3, ITU-R*, 2005.
- [18] A. Rangno (Retiree), "Clouds and fog — classification of clouds," in *Encyclopedia of Atmospheric Sciences (Second Edition)* (G. R. North, J. Pyle, and F. Zhang, eds.), pp. 141–160, Oxford: Academic Press, second edition ed., 2015.
- [19] B. Sklar, *Digital communications: fundamentals and applications*. Pearson, 2021.
- [20] J. E. Gilley, "Digital phase modulation," *Transcrypt International, Inc*, 2003.
- [21] C. A. Ogaja, *Introduction to GNSS Geodesy: Foundations of Precise Positioning Using Global Navigation Satellite Systems*. Springer Nature, 2022.
- [22] S. Cakaj, B. Kamo, V. Koliçi, and O. Shurdi, "The range and horizon plane simulation for ground stations of low earth orbiting (leo) satellites.," *Int. J. Commun. Netw. Syst. Sci.*, vol. 4, no. 9, pp. 585–589, 2011.
- [23] "Earth orbit calculator." <https://www.omnicalculator.com/physics/earth-orbit>, June 2023.
- [24] W. Woodside, "Strings of consecutive successes," *International Journal of Mathematical Education in Science and Technology*, vol. 21, no. 4, pp. 603–605, 1990.
- [25] A. D. Panagopoulos, P.-D. M. Arapoglou, and P. G. Cottis, "Satellite communications at ku, ka, and v bands: Propagation impairments and mitigation techniques," *IEEE communications surveys & tutorials*, vol. 6, no. 3, pp. 2–14, 2004.
- [26] M. R. Soleymani, Y. Gao, and U. Vilaipornsawai, *Turbo coding for satellite and wireless communications*, vol. 702. Springer Science & Business Media, 2006.